

A Learning-based Adaptive Compliance Method for Symmetric Bi-manual Manipulation

Yuxue Cao^{1,*}, Wenbo Zhao^{2,*}, Shengjie Wang^{3,†}, Xiang Zheng⁴,
Wenke Ma⁵, Zhaolei Wang⁶ and Tao Zhang^{2,†} *Fellow, IEEE*

Abstract—Symmetric bi-manual manipulation is an essential skill in on-orbit operations due to its potent load capacity. Previous works have applied compliant control to maintain the stability of manipulations. However, traditional methods have viewed motion planning and compliant control as two separate modules, which can lead to conflicts with the simultaneous change of the desired trajectory and impedance parameters in the presence of external forces and disturbances. Additionally, the joint usage of these two modules requires experts to manually adjust parameters. To achieve high efficiency while enhancing adaptability, we propose a novel Learning-based Adaptive Compliance algorithm (LAC) that improves the efficiency and robustness of symmetric bi-manual manipulation. Specifically, the algorithm framework integrates desired trajectory generation and impedance-parameter adjustment under a unified framework to mitigate contradictions and improve efficiency. Second, we introduce a centralized Actor-Critic framework with LSTM networks preprocessing the force states, enhancing the synchronization of bi-manual manipulation. When evaluated in dual-arm peg-in-hole assembly experiments, our method outperforms baseline algorithms in terms of optimality and robustness.

I. INTRODUCTION

Planning and control of space manipulators play an essential role in on-orbit services, such as assembling and maintaining large space facilities, refueling various space-craft, and establishing extraterrestrial bases [1]. Symmetric bi-manual manipulation is credible for handling objects and performing the peg-in-hole assembly operation, which is essential for the on-orbit assembly of large space facilities or the construction of extraterrestrial bases. Nevertheless, it faces challenges such as inaccurate dynamic models and unsynchronized control of manipulators [2]. Additionally, the environmental contact force interacting with the object must also be considered during manipulation. Therefore, current research commonly combines motion planning and compliance control to achieve the task [3], whereas most of them perform motion planning first and then track the desired trajectory with impedance control. The separate control strategy is inefficient, and the simultaneous changes to these two modules may cause conflicts under certain circumstances. Furthermore, to enhance the robustness of

Our website can be found at <https://sites.google.com/view/lac-manipulation>.

*Equal contribution. †Corresponding author: wangsj23@mails.tsinghua.edu.cn, taozhang@tsinghua.edu.cn.

¹Beijing Institute of Control Engineering, ²Department of Automation, Tsinghua University, ³Institute for Interdisciplinary Information Sciences, Tsinghua University, ⁴Department of Computer Science, City University of Hong Kong, ⁵Qian Xuesen Laboratory of Space Technology, ⁶Beijing Aerospace Automatic Control Institute.

impedance control, some researchers have proposed various optimization methods for selecting impedance parameters online [4], [5], [6], while previous methods need prior information and extra assumptions. Therefore, it remains an open challenge to design a synchronous framework that contains adaptive compliance and motion planning.

In recent years, model-free reinforcement learning (RL) has shown promising results in robot manipulation tasks [7]. We can leverage RL methods to enable a unified framework for motion planning and parameter adjustment tasks, and optimize the planning policy and impedance parameters through interaction experiences. In addition, specific contact dynamics models are unnecessary for model-free methods, eliminating the need for prior information. Compared with single-arm manipulation [8], [9], symmetric bi-manual manipulation requires higher synchronization of dual-arm control, which is particularly important when implementing the cooperative peg-in-hole assembly task. In conclusion, RL-based methods can facilitate symmetric bi-manual manipulation to achieve high efficiency, robustness, and synchronization.

In this paper, we propose the Learning-based Adaptive Compliance (LAC) algorithm for symmetric bi-manual manipulation. The proposed method addresses the synchronous update of both motion planning and compliant control for bi-manual manipulation. Furthermore, it can complete the dual-arm cooperative peg-in-hole assembly operation with a 2mm clearance in which the two arms hold the same peg. The contributions of this paper are as follows:

- We develop a novel algorithm framework to complete symmetric bi-manual manipulation based on RL. The LAC generates the desired trajectory of dual-arm operations, improving motion planning efficiency. Meanwhile, it adaptively updates impedance parameters to overcome the poor robustness of impedance control.
- We design a centralized Actor-Critic network structure to achieve cooperative planning and impedance-parameters modification. The centralization of the framework is useful in operations requiring high dual-arm synchronization. Moreover, results demonstrate that the force trend feature processed by our network greatly improves the performance of compliance operations.
- We verify our method on a typical symmetric bi-manual manipulation task, the dual-arm cooperative peg-in-hole assembly operation. In both simulation environments and real-world settings, the results further validate the feasibility and robustness of the proposed algorithm.

II. RELATED WORK

This section reviews the literature on algorithms that aim to accomplish symmetric bi-manual manipulation.

A. Traditional Methods

In the dual-arm cooperative handling operation, researchers such as Yan [4], Hu [5], and Liu [10] utilized impedance control to manage the manipulators' operating forces. Caccavale proposed a double-loop impedance control method based on the above ideas [11]. In this method, the centralized impedance controller facilitates compliant contact between the object and the environment, while the decentralized impedance controller controls the force between the end-effectors and the object. A host of researchers, including Heck[12] and Tarbouriech[6], further refined the compliant control framework for symmetric bi-manual manipulation based on [11]. Most of the studies cited above utilized manually calibrated impedance parameters, which cannot adapt to changes in the system or environment. Recently, several algorithms that can adjust impedance parameters online have been proposed, such as those based on nonlinear optimization [13], quadratic optimization [4], adaptive law compensation [14], and neural network [15]. While these methods consider the control of internal and external forces, it is currently only applied to dual-arm cooperative handling operations. Though there are several studies on the single-arm peg-in-hole assembly [16], [17], research on dual-arm assemblies is scarce and mainly involves unsymmetrical cooperative operations, where one arm holds the peg and the other holds the hole [18]. To our knowledge, there is no published research on the symmetrical dual-arm peg-in-hole assembly operation, where both arms hold the same peg.

B. Reinforcement Learning Methods

Model-free reinforcement learning was initially used for single-arm compliant operations, where Stulp et al. used the PI^2 algorithm to learn variable impedance, adapting to both deterministic and stochastic force fields [19]. With the development of neural networks, Beltran-Hernandez applied reinforcement learning to single-arm peg-in-hole assembly, which utilized TCN and MLP networks to pre-process observations [20]. Several references, including [21], [22], [23], [9], focused on adjusting impedance parameters to reduce the contact force between the peg and the hole and the assembly time. While reinforcement learning has made remarkable achievements in single-arm operations, few studies have focused on dual-arm operations. Alles and Al-jalbout proposed a reinforcement learning framework with a centralized policy network and two decentralized single-arm controllers [24]. Its effectiveness was verified in the asymmetric peg-in-hole assembly. However, as far as we know, no study has yielded the effect of reinforcement learning in symmetric bi-manual manipulation with strong kinematics and dynamics constraints. The closed-chain system requires higher synchronization of dual-arm control, which brings new challenges to the application of reinforcement learning.

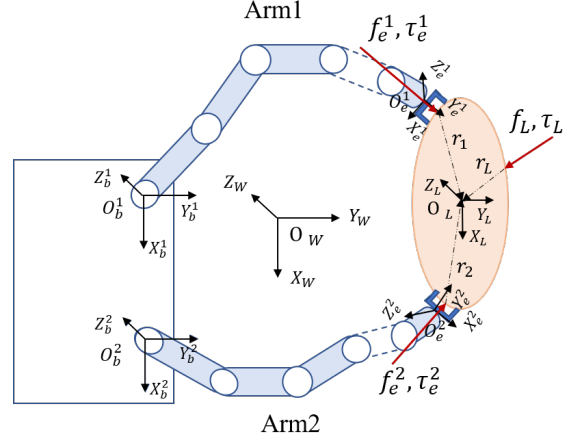


Fig. 1: Closed-chain model of the dual-arm robot.

III. PROBLEM FORMULATION

A. Kinematic and Dynamic Model of the Dual-Arm Closed-Chain System

1) *Kinematic Model*: To maintain a stable connection between the end-effectors and the object, the whole movement process must comply with the closed-chain kinematics constraints formulated as follows:

$$T_{e^i}^{b^i} = T_W^{b^i} T_L^W T_{e^i}^L \quad (1)$$

where T_A^B represents the transformation matrix of the coordinate system A relative to the coordinate system B .

2) *Dynamic model*: In Fig. 1, f_L and τ_L are the external force and moment exerted on the object by the environment. f_e^i and τ_e^i are the force and moment applied to the object by the i -th manipulator. r_L , r_1 , r_2 are vectors from the force points of f_L , f_e^1 , f_e^2 to the object's centroid. v_L and w_L are the velocity and angular velocity of the object. M_L , I_L and G_L are the object's mass, moment of inertia and gravity, respectively. The dynamic model of the dual-arm closed-chain system can be formulated as:

$$\begin{bmatrix} I_3 & O \\ (r_1)^* & I_3 \end{bmatrix} \begin{bmatrix} f_e^1 \\ \tau_e^1 \end{bmatrix} + \begin{bmatrix} I_3 & O \\ (r_2)^* & I_3 \end{bmatrix} \begin{bmatrix} f_e^2 \\ \tau_e^2 \end{bmatrix} + \begin{bmatrix} G_L \\ O \end{bmatrix} + \begin{bmatrix} I_3 & O \\ (r_L)^* & I_3 \end{bmatrix} \begin{bmatrix} f_L \\ \tau_L \end{bmatrix} = \begin{bmatrix} m_L \dot{v}_L \\ I_L \dot{\omega}_L + \omega_L \times (I_L \omega_L) \end{bmatrix} \quad (2)$$

where $(\cdot)^*$ represents the transpose of the vector. Eq. 2 can be simplified as $-\Gamma_1 F_e^1 - \Gamma_2 F_e^2 = -\bar{G}_L - \Gamma_L F_L + F_{IL}$, where the generalized force F represents the vector composed of force and moment. Since the motion planning algorithms generate the desired trajectory for the object, and in turn determines F_{IL} , the primary challenge of this problem is to decompose that of the object's centroid into the desired generalized forces of the end-effectors. This paper refers to the shared force mode proposed in [25], obtaining the desired generalized forces of the end-effectors as follows:

$$\begin{bmatrix} F_e^1 \\ F_e^2 \end{bmatrix} = [-\Gamma_1 \quad -\Gamma_2]^\# (-\bar{G}_L - \Gamma_L F_L + F_{IL}) \quad (3)$$

where $\#$ represents the pseudo inverse of the matrix.

B. Position-based Impedance Control

The position-based impedance control converts force errors into position adjustment, and realizes force control by adjusting the desired trajectory. The second-order dynamic model between force and position is:

$$M_d(\ddot{X} - \ddot{X}_d) + B_d(X - \dot{X}_d) + K_d(X - X_d) = F - F_d \quad (4)$$

where M_d , B_d and K_d are the positive definite matrices of desired inertia, damping and stiffness of the impedance model, respectively. Diagonal matrices are usually selected to obtain the linear decoupling response. \ddot{X} , \dot{X} , X represent the actual acceleration, velocity and position, respectively. \ddot{X}_d , \dot{X}_d , X_d are the desired acceleration, velocity and position. F_d and F are the desired and the actual contact force, respectively.

The Lagrangian transformation and discretization are applied to Eq. 4 to deduce position adjustment from force errors, as Eq. 5 shows.

$$\begin{aligned} \delta X(t) = & \frac{T^2}{\omega_1} (E(t) + 2E(t-1) + E(t-2)) - \\ & \frac{\omega_2}{\omega_1} \delta X(t-1) - \frac{\omega_3}{\omega_1} \delta X(t-2) \end{aligned} \quad (5)$$

where $E(t) = F(t) - F_d(t)$, and T is the sampling period. $\omega_1 = 4M_d + 2B_dT + K_dT^2$, $\omega_2 = -8M_d + 2K_dT^2$, and $\omega_3 = 4M_d - 2B_dT + K_dT^2$. Then the actual trajectory at time t can be calculated as: $X(t) = X_d(t) + \delta X(t)$.

IV. ADAPTIVE COMPLIANCE ALGORITHM BASED ON REINFORCEMENT LEARNING

A. Reinforcement Learning

The process of reinforcement learning can be described as a Markov decision process (MDP). The MDP process comprises five components: $\langle S, A, R, P, \rho_0 \rangle$. The agent gets the environment state $s_t \in S$ and generates the action $a_t \in A$ using the current policy $\pi(s_t)$. Once a_t is performed, the environment transitions to a new state s_{t+1} , and the agent obtains a reward r_t . Reinforcement learning endeavors to find the optimal policy π^* that yields the maximum expected reward value. For this paper, we utilize the Soft Actor-Critic (SAC) algorithm [26]. Unlike other deep reinforcement learning algorithms, SAC takes into account both the reward value and policy entropy maximization. Maximizing policy entropy facilitates the exploration of policy, thereby allowing the algorithm to find the optimal solution more effectively in high-dimensional optimization problems.

B. Workflow of Symmetric Bi-manual Manipulation

In this paper, we extend the double-loop impedance method proposed in [11] and adapt it to symmetric bi-manual manipulation. The manipulation workflow is illustrated in Fig. 2, which comprises three parts. After the motion planning model generates the object's desired trajectory, denoted as X_d^o , the outer impedance adjusts the object's position to minimize the external force, denoted as F_{env} ,

which the environment exerts on the object. The second-order impedance model can be rewritten as Eq. 6 for the outer impedance.

$$M_d^o \ddot{X}_e^o + B_d^o \dot{X}_e^o + K_d^o X_e^o = F_{env} \quad (6)$$

where $X_e^o = X_o - X_d^o$ is the adjustment to the object's desired trajectory X_d^o . After obtaining X_e^o through Eq. 6, we can compute the compliant object trajectory X_o by adding X_e^o and X_d^o . The compliant desired trajectory X_o decreases the interactive environmental force.

The second part pertains to the dual-arm closed-chain kinematics and dynamics model. This part calculates the desired trajectory X_d^i and the desired force F_d^i of the manipulator according to Eq. 1 and Eq. 3, respectively.

Once X_d^i and F_d^i are calculated, the inner impedance and single-arm control are implemented to drive the motion of manipulators. The inner loop's second-order impedance model is formulated as:

$$M_d^i \ddot{X}_e^i + B_d^i \dot{X}_e^i + K_d^i X_e^i = F_e^i \quad (7)$$

where $X_e^i = X_i - X_d^i$ is the adjustment to the desired trajectory of the i -th manipulator's end-effector X_d^i . $F_e^i = F_d^i - F_i$ is the error between the end-effector's desired force and the actual contact force.

C. Learning-based Adaptive Compliance(LAC) Algorithm

We design an adaptive compliance algorithm based on reinforcement learning, which aims to enhance the efficiency of motion planning and bi-manual manipulation compliance.

1) *Algorithm Framework*: As shown in Fig. 2(b), the framework of our proposed learning-based adaptive compliance method for symmetric bi-manual manipulation is a centralized framework comprising two components. The high-level module, which runs reinforcement learning at a fixed frequency of 20 Hz, provides the object's desired trajectory and impedance parameters. Additionally, it acquires the states of two manipulators simultaneously. On the other hand, the low-level module involves impedance control operating at a frequency much higher than the high-level module. The slow control frequency of high-level reinforcement learning allows the agent to process environmental states and generate the next action, while the high frequency of the low-level module ensures precise and prompt control of the manipulators.

The reinforcement learning policy outputs $\{a_x, a_p\}$, where $a_x = [\Delta x, \Delta y, \Delta z] \in R^3$ corresponds to the object's position change and represents the motion planning module, and $a_p = [B_d, K_d] \in R^6$ corresponds to the desired damping matrix and stiffness matrix diagonal values of the impedance controller. The desired inertia matrix remains constant because it significantly affects the system's stability. Furthermore, to maintain the control system's stability, the impedance parameters' upper and lower limits are defined as hyper-parameters of the algorithm, a_p^{max} and a_p^{min} , respectively. In the low-level module, the impedance controller with variable parameters modifies the desired trajectory X_d output by the policy, resulting in compliant operations.

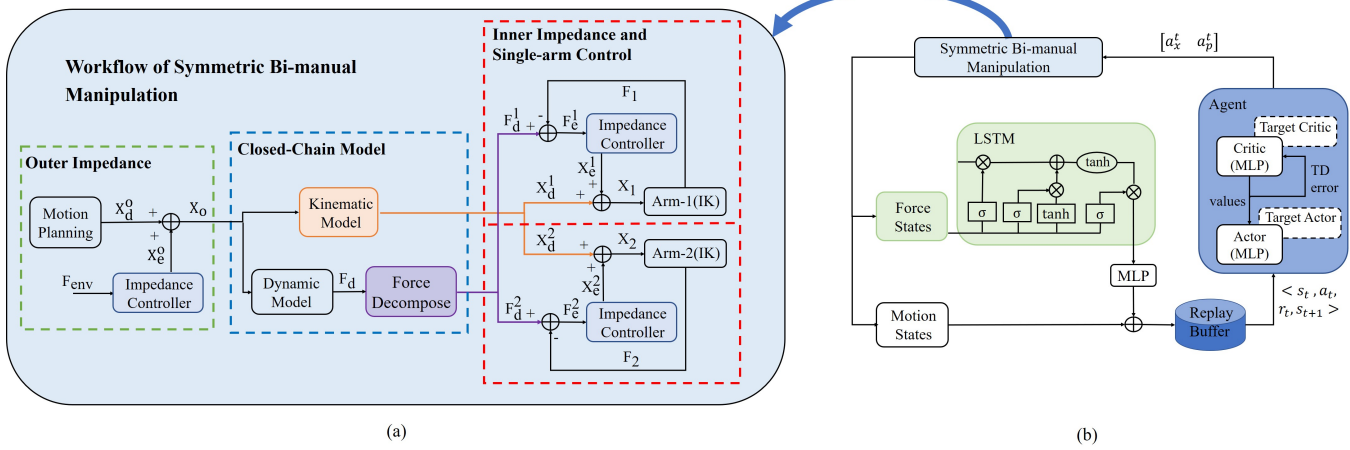


Fig. 2: Algorithm framework of LAC. (a) Workflow of symmetric bi-manual manipulation consists of three parts. (b) Adaptive compliance algorithm based on reinforcement learning.

2) *Neural Network Architecture*: As the environmental states s_t are divided into motion states m_t and force states f_t , the manipulator's motion constraints limit the change rate of m_t , and the states between two moments have strong continuity. Nevertheless, f_t are related to current contact dynamics and hence show intense volatility. Moreover, adjusting the sub-goal position and impedance parameters should consider the current force information and its trend. Therefore, we enable the agent to obtain the force states at the low-level frequency to enhance the states' continuity and promote better algorithm performance. Since Long Short-Term Memory (LSTM) establishes connections between nodes of different hidden layers and can use past moments' information to infer the future moment's state, we utilize LSTM networks to the original deep reinforcement learning MLP network architecture, intending to process the force states sequence. A fully connected layer then processes the output of the LSTM networks to obtain the feature vector of the force states. After that, the motion states are connected with the pre-processed force feature vector, which is then input into the agent's neural networks. The algorithm pseudo-code of our approach is available in Algorithm 1.

D. Dual-arm Cooperative Peg-in-hole Assembly

Fig. 3 depicts the simulation environment of the dual-arm cooperative peg-in-hole assembly operation. The agent's observations include end-effectors' poses $P_e^{1,2}, \Phi_e^{1,2} \in R^6$, velocities $v_e^{1,2}, \omega_e^{1,2} \in R^6$, and the pose of the object's centroid $P_o, \Phi_o \in R^6$. Additionally, the error vector between the current position and the target position of the object is included in the state space to enhance learning efficiency. Note that the algorithm primarily focuses on the interaction states between the peg and hole during assembly, and as a result, the state space omits the manipulators' joint information. Additionally, the state space includes the contact force between the peg and the hole ($F_{env} \in R^3$) and the peg insertion depth (d). The policy outputs the object's centroid positional variation $[\Delta x, \Delta y, \Delta z]$, as well

as the desired damping $B_d^o \in R^3$ and stiffness $K_d^o \in R^3$ of the outer impedance controller. Furthermore, to improve learning efficiency in dual-arm assembly, we adopt a hybrid policy that leverages the knowledge of the PD position error controller. The object's desired trajectory (X_d^o) is the sum of the PD position controller's output (X_g) and the reinforcement learning policy's output (a_x), expressed as $X_d^o = X_g + a_x$. The hybrid policy accelerates the search process before the peg contacts the hole.

As for the reward function, the peg's insertion depth is the primary indicator of successful assembly. Additionally, minimizing the interaction force between the peg and hole reduces wear between parts during insertion. However, to prevent the agent from avoiding insertion, we decrease the weight of contact force in the reward function. Completion time is another performance indicator. The reward value increases as the completion time shortens, encouraging the agent to complete the task quickly. Therefore, the reward function is structured as follows.

$$r = \begin{cases} 1.05 - \tanh(d) - 0.05 \times \tanh(F_{env}), & F_{env} \leq F_{max} \\ 100 + ((1 - t/T) \times 100), & d \geq d_s \\ -10, & \text{Not safe} \end{cases} \quad (8)$$

where d_s is the target insertion depth. When safety problems occur, we will penalize the agent with -10 and terminate the current episode. The safety problems include two aspects: 1) the interaction force between the peg and the hole exceeds the defined threshold F_{max} ; 2) the closed-chained constraint is not satisfied during the assembly process, causing the object to fall away.

V. SIMULATION RESULTS AND REAL WORLD EXPERIMENTS

A. Simulation Environment and Real-World Settings

We first build simulation environments for the dual-arm cooperative peg-in-hole assembly task using Mujoco, a widely used simulation platform in reinforcement learning.

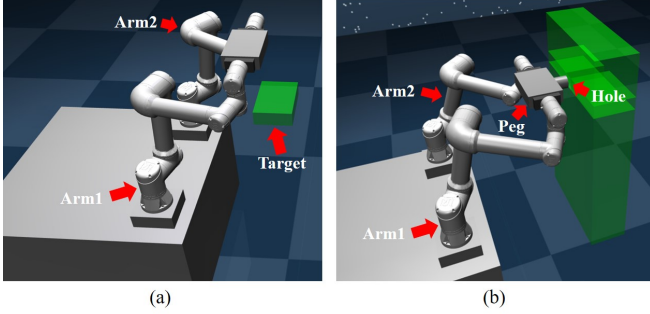


Fig. 3: The two stages of the dual-arm cooperative peg-in-hole assembly task. The object needs to be first transported to the target position and then slowly inserted.

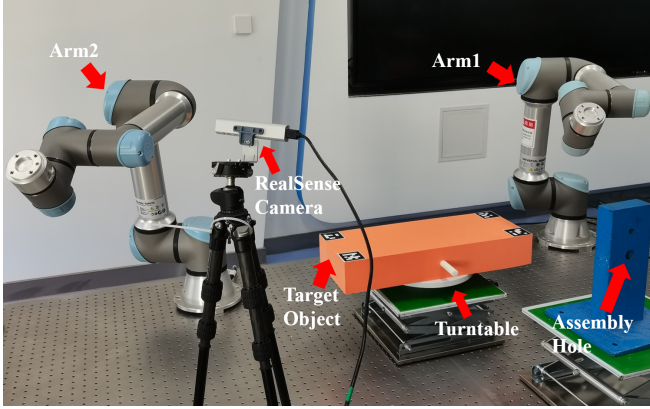


Fig. 4: The ground-based dual-arm robot system for typical on-orbit assembly operation.

The target position of the object's centroid is located in a $[0.1m, 0.3m, 0.12m]$ cube. The hyperparameters of **LAC** are illustrated in Table I.

To further validate the proposed algorithm, we construct a ground-based dual-arm robot system for typical on-orbit assembly operations, as shown in Fig. 4. The whole system mainly consists of two six-DoF UR robot arms, a target object, a turntable, an assembly hole, a RealSense camera and a laptop computer. The laptop serves as the master computer for the two UR robot arms, running the dual-arm cooperative motion planning algorithm and the compliant control algorithm and sending the desired joint angles to the joint controllers of each arm via TCP/IP protocol. During the experiment, the data required by the master computer is estimated by the RealSense camera, which are used as inputs of a pre-trained reinforcement learning policy network. The framework of the real-world system is shown in Fig. 5.

We argue that our algorithm's performance improvement depends on four key factors: using SAC as reinforcement learning algorithm which takes policy entropy into account, introducing impedance mechanism into the closed-chain dual-arm system, variable impedance parameters, and pre-processing force states with LSTM networks. We provide the abbreviation of each algorithm: the algorithm with **TD3**, the algorithm only using RL training without impedance

TABLE I: Hyperparameters of **LAC**

Hyperparameters	LAC
LSTM/MLP network	16/3 (256,256)
Actor network	(256,256)
Critic network	(256,256)
Learning rate of actor	1.e-3
Learning rate of critic	5.e-4
Optimizer	Adam
ReplayBuffer size	10^6
Discount (γ)	0.995
Polyak ($1 - \tau$)	0.995
Batch size	128
Length of an episode	200 steps
Maximum steps	1e6 steps

controller (**SAC**), the algorithm with fixed impedance parameters (**LAC w/ fixed Imp**) and the algorithm without LSTM networks (**LAC w/o LSTM**).

B. Dual-arm Cooperative Assembly

1) *Ablation Studies*: Fig. 6 depicts the average reward curve during the training of different algorithms under the dual-arm cooperative assembly scenario. The shaded regions correspond to the standard deviation using three different random seeds. Our algorithm displays a more stable and larger convergence value compared to the others. The low reward value of **TD3** implies that it is hard to find a satisfactory policy for the assembly task without enough exploration. The reward value of **SAC** increases initially but declines rapidly and ultimately maintains a low value, which indicates that the interaction force between the peg and the hole exceeds the acceptable range without outer impedance and the training process fails. As **LAC w/ fixed Imp** has a lower action space dimension with only the position change outputs, and **LAC w/o LSTM** does not need to learn the parameters of LSTM networks, the reward values of these two algorithms rise more rapidly than **LAC** at the initial stage. However, **LAC w/ fixed Imp** cannot real-time adjust the impedance relationship between the peg and the hole, and **LAC w/o LSTM** only considers the current force rather than the trend of force change. Thus, their average reward values fluctuate violently during the training.

After training, we test the training results on the same scenario. The cyan line in Fig. 7 shows the peg insertion depth during the assembly in the simulation environment, and the noted lines in Fig. 8 show the contact force error between the peg and the hole in the same scenario. The plot indicates that collision occurs between the peg and the hole when $timestep = 30$. However, with the outer impedance control, the contact force on the X-axis (the impact direction) rapidly decreases, and the peg continues to insert into the hole. The contact forces on the X and Z axes remain within a small range throughout the insertion. In the final insertion stage, the force on the Y-axis notably increases at $timestep = 90$, but it decreases from $timestep = 110$ with the adjustment of **LAC**. The peg eventually reaches the target insertion depth at $timestep = 123$.

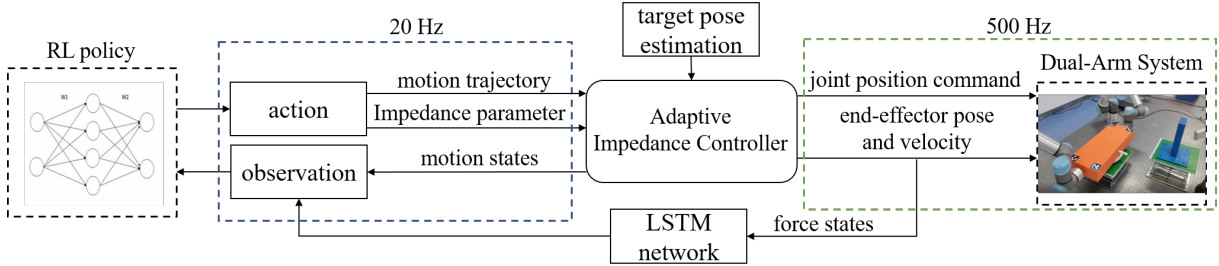


Fig. 5: Block diagram of experimental system of adaptive compliance control algorithm based on reinforcement learning.

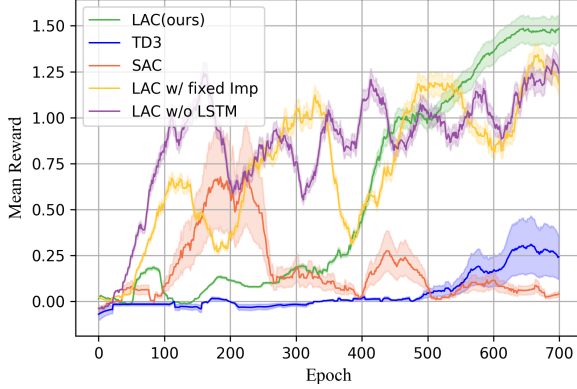


Fig. 6: Mean reward curve during the training of different algorithms for the dual-arm peg-in-hole assembly operation (Curves smoothed report the mean of 3 times, and shadow areas show the variance.).

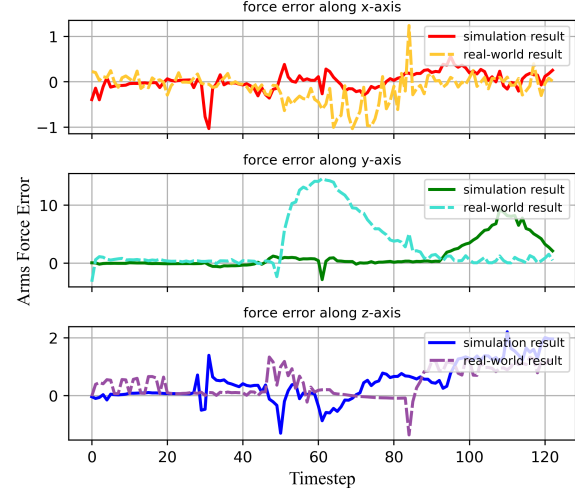


Fig. 8: The contact force error bewteen the peg and the hole during the assembly in the simulation environment and real-world experiment.

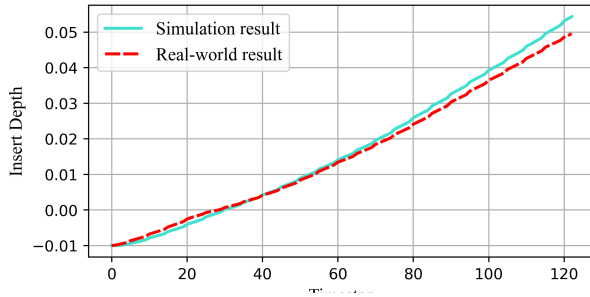


Fig. 7: The peg insertion depth during the assembly in the simulation environment and real-world experiment.

2) *Evaluation of the Generalization:* We design two test scenarios in the simulation environment to verify the generalization of our algorithm in dual-arm cooperative peg-in-hole assembly. Given the poor performance of **TD3** and **SAC**, we only compare our algorithm with the other two algorithms, named **LAC w/ fixed Imp** and **LAC w/o LSTM**.

The first scenario is to verify the effectiveness of **LAC** in the presence of a position error in the assembly environment. Specifically, a random error ranging from 1mm to 5mm is added to the hole centre on the y-z plane. In 20 test experiments, our algorithm has the highest number of successful attempts (18), followed by **LAC w/o LSTM**.

(14), and **LAC w/ fixed Imp** with the minimum (13). Fig. 9 visually shows the mean and standard deviation of the three algorithms on the maximum environmental contact force and assembly steps. The results indicate that our method better balances assembly speed and contact force. Although the average assembly time of **LAC w/o LSTM** is slightly lower than ours, the average contact force it generated is larger. On the other hand, the average maximum contact force and assembly time of **LAC w/ fixed Imp** are the largest because it cannot adjust impedance parameters.

The other scenario is to test the adaptability of our algorithm in various material environments. Table II and Table III display the maximum environmental contact force and assembly steps of different algorithms in varying stiffness and damping test environments. The tables show that the variable impedance has excellent adaptability in large stiffness environments. In comparison, the maximum contact force of **LAC w/ fixed Imp** exceeds the specified safety threshold and cannot complete assembly operation in large stiffness environments. All three algorithms show an increase in maximum contact force in environments with large damping. Our algorithm's assembly steps demonstrate remarkable

Algorithm 1 Learning-based Adaptive Compliance(LAC)

```

1: Randomly initialize the parameters of the state pre-
   process networks (including LSTM, MLP); randomly
   initialize the agent's actor network with  $l_a, w_a, \phi$  and
   critic network with  $l_c^i, w_c^i, \theta_i$ , where  $i = 1, 2$ 
2: Initialize replay buffer  $\mathcal{D}$ , the frequency of the high-level
   module  $h_h$  and low-level module  $h_l$ 
3: Initialize the parameters of target network with
    $l_c^{i'}, w_c^{i'}, \theta_i' \leftarrow l_c^i, w_c^i, \theta_i, i = 1, 2$ 
4: for episode  $e = 1, \dots, E$  do
5:   Sample initial state  $s_0$ 
6:   for step  $t = 0, \dots, T - 1$  do
7:     Divide  $s_t$  into  $m_t$  and  $f_t$ , input  $f_t$  into LSTM
       networks to get the force feature vector  $v_t$ 
8:     Combine  $m_t$  with  $v_t$  to obtain the feature vector  $c_t$ 
9:     Sample an action  $a_t = \{a_x^t, a_p^t\}$  from  $\pi_\phi(a_t|c_t)$ 
10:    for step  $u = 0, h_l/h_h - 1$  do
11:      if outer impedance then
12:        Set outer impedance parameters to be  $a_p^t$ , and
           use  $a_x^t$  to calculate  $X_o$  according to Eq.6
13:        Use  $X_o$  to calculate  $X_d^i$  and  $F_d^i$  of the end-
           effectors according to Eq.1 and Eq.3
14:      else if inner impedance then
15:        Use  $a_x^t$  to calculate  $X_d^i$  and  $F_d^i$  of the end-
           effectors according to Eq.1 and Eq.3
16:        Set inner impedance parameters to be  $a_p^t$ 
17:      end if
18:      Calculate  $X_i$  according to Eq.7, and convert it
           to the desired joint angles  $q_{d,i}^u$  to control the
           manipulator
19:    end for
20:    observe a new state  $s_{t+1}$  and store
        $\langle s_t, a_t, r_t, s_{t+1} \rangle$  into  $\mathcal{D}$ 
21:  end for
22:  for iteration  $n = 1, N$  do
23:    Sample a minibatch  $\mathcal{B}$  from replay buffer  $\mathcal{D}$ 
24:    Update critic network  $l_c^i, w_c^i, \theta_i, i = 1, 2$  using
       minibatch  $\mathcal{B}$ 
25:    Update actor network  $l_a, w_a, \phi$  using minibatch  $\mathcal{B}$ 
26:    Soft update the parameters of target networks,
        $l_c^{i'}, w_c^{i'}, \theta_i', i = 1, 2$ 
27:  end for
28: end for

```

stability in different environments, while the assembly steps of the other two algorithms increase to varying degrees.

3) *Real-World Experiments*: We conduct the real-world peg-in-hole experiment based on the dual-arm collaborative handling operation. Among 20 shaft hole assembly testing experiments, the LAC algorithm succeeded the task 17 times totally. In the successful experiments, the average maximum contact force of the target object was 19.718N, and the average assembly time was 141 time steps (7.05s). The screenshots of the physical experiment process of the real-

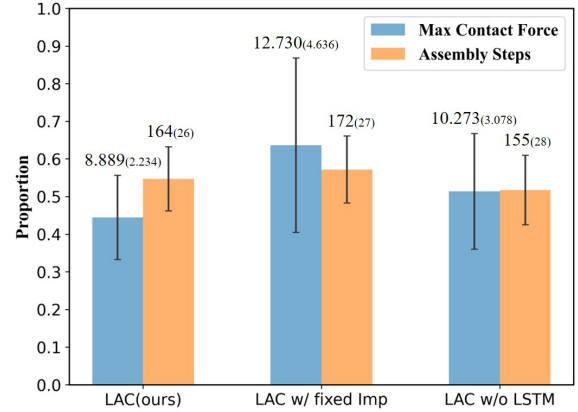


Fig. 9: Mean and standard deviation of the maximum environmental contact force and assembly steps in the test environment with a random error ranging from 1mm to 5mm of the hole centre on the y-z plane.

TABLE II: Max contact force of different algorithms in different stiffness and damping test environments.

Algorithms	$K_l, B_l/N$	$K_l, B_s/N$	$K_s, B_l/N$	$K_s, B_s/N$
LAC(ours)	12.776	5.454	13.668	3.260
LAC w/ fixed Imp	27.366	21.812	13.962	8.815
LAC w/o LSTM	14.447	7.063	14.620	7.597

TABLE III: Assembly steps of different algorithms in different stiffness and damping test environments.

Algorithms	K_l, B_l	K_l, B_s	K_s, B_l	K_s, B_s
LAC(ours)	124	128	127	123
LAC w/ fixed Imp	None	None	201	127
LAC w/o LSTM	142	138	147	130

world dual-arm collaborative peg-in-hole task are shown in Fig. 10. The red line in Fig. 7 shows the insertion depth of the shaft, and the noted lines in Fig. 8 show the interaction force during the assembly process. Through the contrast of the simulation results and real-world experiment results under exactly the same parameter settings, it is obvious that the corresponding lines are highly similar, which indicates that our proposed method can be easily generalized to real-world environments with high precision and robustness. In Fig. 8, the assembly shaft and the hole come into contact at $timestamp = 47(t = 2.35s)$, and the contact force along the Y-axis increases during the insertion process. However, with the adjustment of the outer loop impedance controller, this error gradually decreases from $timestamp = 62(t = 3.1s)$ and eventually fluctuates around zero. Throughout the insertion process, the contact force along the X-axis and Z-axis remains within a small range. The insertion depth of the assembly shaft reaches the target depth at $timestamp = 132(t = 6.6s)$. The experimental results show that our proposed algorithm can achieve high-precision dual-arm assembly task within a safe range of interaction forces.

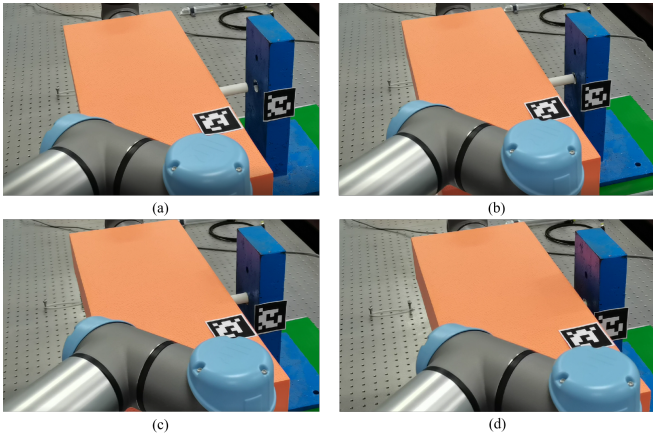


Fig. 10: Real-World dual-arm assembly task. (a) Initial state of the system. (b) (c) The shaft is being inserted in the assembly hole. (d) The shaft achieves the target depth.

VI. CONCLUSUIN

The current framework for symmetric bi-manual manipulation performs motion planning first and then tracks the desired trajectory with a compliance controller, which is inefficient and may cause conflicts between the two modules. Furthermore, due to the difficulty in establishing contact dynamics and the high requirements for dual-arm synchronous control, no research has particularly focused on the dual-arm cooperative peg-in-hole operation. To address these challenges, we propose the Learning-based Adaptive Compliance (LAC) algorithm, which incorporates the advantages of reinforcement learning to improve the flexibility, adaptability, and robustness in symmetric bi-manual manipulation. Simulation results demonstrate that the proposed algorithm facilitates dual-arm cooperative control with considerable environmental adaptability in high-precision assembly operations. Real-world experiments further verify the proposed method and show the high robustness and strong generalization ability of the algorithm.

REFERENCES

- [1] Zhihong Jiang, Xiaolei Cao, Xiao Huang, Hui Li, and Marco Cecarelli. Progress and development trend of space intelligent robot technology. *Space: Science & Technology*, 2022.
- [2] Yun-Hua Wu, Zhi-Cheng Yu, Chao-Yong Li, Meng-Jie He, Bing Hua, and Zhi-Ming Chen. Reinforcement learning in dual-arm trajectory planning for a free-floating space robot. *Aerospace Science and Technology*, 98:105657, 2020.
- [3] D. Surdilovic. Synthesis of impedance control laws at higher control levels: algorithms and experiments. In *IEEE International Conference on Robotics & Automation*, 1998.
- [4] Lei Yan, Yiming Yang, Wenfu Xu, and Sethu Vijayakumar. Dual-arm coordinated motion planning and compliance control for capturing moving objects with large momentum. In *2018 IEEE/RSJ International Conference on Intelligent Robots and Systems (IROS)*, pages 7137–7144, 2018.
- [5] Bingshan Hu, Lei Yan, Liangliang Han, and Hongliu Yu. Coordinated compliance control of dual-arm robot astronaut for payload operation. *International Journal of Advanced Robotic Systems*, 18(3):20–28, 2021.
- [6] Sonny Tarbouriech, Benjamin Navarro, Philippe Fraisse, Andre Crosnier, Andrea Cherubini, and Damien Salle. Admittance control for collaborative dual-arm manipulation. pages 198 – 204, 2019.
- [7] Hao Ju, Rongshun Juan, Randy Gomez, Keisuke Nakamura, and Guangliang Li. Transferring policy of deep reinforcement learning from simulation to reality for robotics. *Nature Machine Intelligence*, 4(12):1077–1087, 2022.
- [8] Shir Kozlovsky, Elad Newman, and Miriam Zackenhouse. Reinforcement learning of impedance policies for peg-in-hole tasks: Role of asymmetric matrices. *IEEE Robotics and Automation Letters*, 7(4):10898–10905, 2022.
- [9] Masahide Oikawa, Tsukasa Kusakabe, Kyo Kutsuzawa, Sho Sakaino, and Toshiaki Tsuji. Reinforcement learning for robotic assembly using non-diagonal stiffness matrix. *IEEE Robotics and Automation Letters*, 6(2):2737–2744, 2021.
- [10] Xuefei Liu, Xiangrong Xu, Zuojun Zhu, and Yanglin Jiang. Dual-arm coordinated control strategy based on modified sliding mode impedance controller. *Sensors*, 21(14), 2021.
- [11] Fabrizio Caccavale, Pasquale Chiachio, Alessandro Marino, and Luigi Villani. Six-dof impedance control of dual-arm cooperative manipulators. *IEEE/ASME Transactions on Mechatronics*, 13(5):576–586, 2008.
- [12] Dennis Heck, Dragan Kosti, Alper Denasi, and Henk Nijmeijer. Internal and external force-based impedance control for cooperative manipulation. pages 2299 – 2304, 2013.
- [13] Mantian Li, Kun Li, Pengfei Wang, Yizhou Liu, Fusheng Zha, and Wei Guo. Indirect adaptive impedance control for dual-arm cooperative manipulation. In *2017 2nd International Conference on Advanced Robotics and Mechatronics (ICARM)*, pages 650–655, 2017.
- [14] Chunting JIAO, Xiong WEI, Han ZHAO, and Xiaojie SU. Adaptive hybrid impedance control for a dual-arm robot manipulating an unknown object. In *IECON 2020 The 46th Annual Conference of the IEEE Industrial Electronics Society*, pages 2754–2759, 2020.
- [15] Ningjing Zheng, Liang Han, and Wenfu Xu. A dual-arm cooperative manipulator: Modularized design and coordinated control. In *2018 IEEE International Conference on Information and Automation (ICIA)*, pages 945–950, 2018.
- [16] Yuhang Gai, Jiuming Guo, Dan Wu, and Ken Chen. Feature-based compliance control for precise peg-in-hole assembly. *IEEE TRANSACTIONS ON INDUSTRIAL ELECTRONICS*, 69(9):9309–9319, SEP 2022.
- [17] Hyeonjun Park, Jaeheung Park, Dong-Hyuk Lee, Jae-Han Park, and Ji-Hun Bae. Compliant peg-in-hole assembly using partial spiral force trajectory with tilted peg posture. *IEEE ROBOTICS AND AUTOMATION LETTERS*, 5(3):4447–4454, JUL 2020.
- [18] Yanjiang Huang, Yanglong Zheng, Nianfeng Wang, Jun Ota, and Xianmin Zhang. Peg-in-hole assembly based on master-slave coordination for a compliant dual-arm robot. *Assembly Automation*, 40, 2020.
- [19] Freek Stulp, Jonas Buchli, Alice Ellmer, Michael Mistry, Evangelos A. Theodorou, and Stefan Schaal. Model-free reinforcement learning of impedance control in stochastic environments. *IEEE Transactions on Autonomous Mental Development*, 4(4):330–341, 2012.
- [20] Cristian Camilo Beltran Hernandez, Damien Petit, Ixchel G. Ramirez-Alpizar, and Kensuke Harada. Variable compliance control for robotic peg-in-hole assembly: A deep reinforcement learning approach. 2020.
- [21] Patrick Varin, Lev Grossman, and Scott Kuindersma. A comparison of action spaces for learning manipulation tasks. In *2019 IEEE/RSJ International Conference on Intelligent Robots and Systems (IROS)*, pages 6015–6021, 2019.
- [22] Fengming Li, Qi Jiang, Sisi Zhang, Meng Wei, and Rui Song. Robot skill acquisition in assembly process using deep reinforcement learning. *Neurocomputing*, 345:92 – 102, 2019.
- [23] Fengming Li, Qi Jiang, Wei Quan, Rui Song, and Yibin Li. Manipulation skill acquisition for robotic assembly using deep reinforcement learning. In *2019 IEEE/ASME International Conference on Advanced Intelligent Mechatronics (AIM)*, pages 13–18, 2019.
- [24] Marvin Alles and Elie Aljalbout. Learning to centralize dual-arm assembly. 2021.
- [25] Lei Yan, Zonggao Mu, Wenfu Xu, and Bingsong Yang. Coordinated compliance control of dual-arm robot for payload manipulation: Master-slave and shared force control. In *2016 IEEE/RSJ International Conference on Intelligent Robots and Systems (IROS)*, pages 2697–2702. IEEE, 2016.
- [26] Tuomas Haarnoja, Aurick Zhou, Pieter Abbeel, and Sergey Levine. Soft actor-critic: Off-policy maximum entropy deep reinforcement learning with a stochastic actor. In *International conference on machine learning*, pages 1861–1870. PMLR, 2018.